Electronic Supplementary Material (ESI) for Nanoscale Advances.

Supplementary information

S1 Crystallinity characterization of the single layer graphene.

The single layer graphene was grown by CVD method on commercial copper foil, produced by GoodFellow.

Figure S1-1 shows the XRD spectrum of GoodFellow copper foil after the synthesis process.

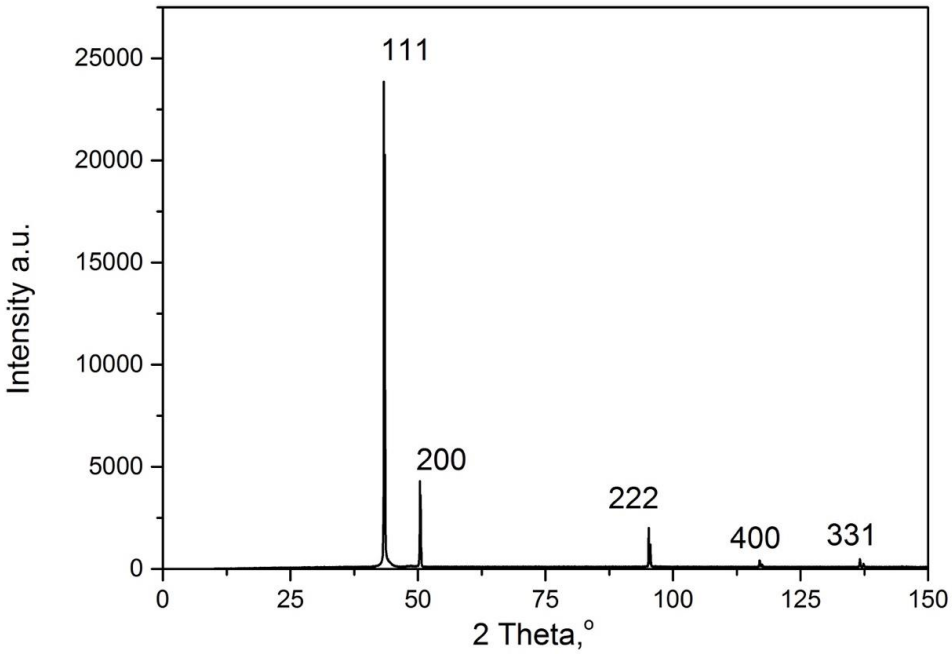

Figure S1-1. XRD spectrum of GoodFellow copper foil after graphene synthesis.

In table S1 Miller indexes and relative intensities of reflexes for ideal polycrystalline copper face-centered cubic (fcc) structure and those observed in our experiment are presented.

Table S1. Miller indexes allowed in fcc structure. Relative intensities for ideal copper and for the GoodFellow copper foil after the graphene synthesis.

Miller indexes ***h k l***	Relative intensities in %	
	Ideal copper	*Our experiment*
1 1 1	100	100
2 0 0	46	19
2 2 0	20	Not observable
3 1 1	17	Not observable
2 2 2	5	8
4 0 0	3	1.7
3 3 1	9	2.3
4 2 0	8	Not observable

The absence of some reflections in XRD spectra together with significant difference in the relative intensity of observed reflexes with polycrystalline ideal copper allow to conclude that the copper foil is highly but not fully oriented, with dominant 111 reflection, (1 1 1) plane is parallel to the foil surface. However, the in-plane orientation of (1 1 1) terminated grains at the surface copper foil needs additional studies (for example Electron backscatter diffraction (EBSD) analysis) and are beyond of the scope of this work.

To study the crystallinity of the graphene transferred to SiO_2/Si substrate the reflection high energy electron diffraction (RHEED) technique was applied. Figure S1-2 shows RHEED pattern observed at different azimuthal angels. The RHEED pattern is the result of the intersection of the Ewald sphere and one-dimensional roads forming hexagonal reciprocal lattice of graphene. The intensity profiles marked by «k_y – direction» are taken along the blue lines for each pattern, whereas for the «k_x – direction» they are taken along the red lines. No oscillation in «k_y – direction» profile reveals that graphene is mostly single layer which correlates with the Raman and transparency data (see SI S2).

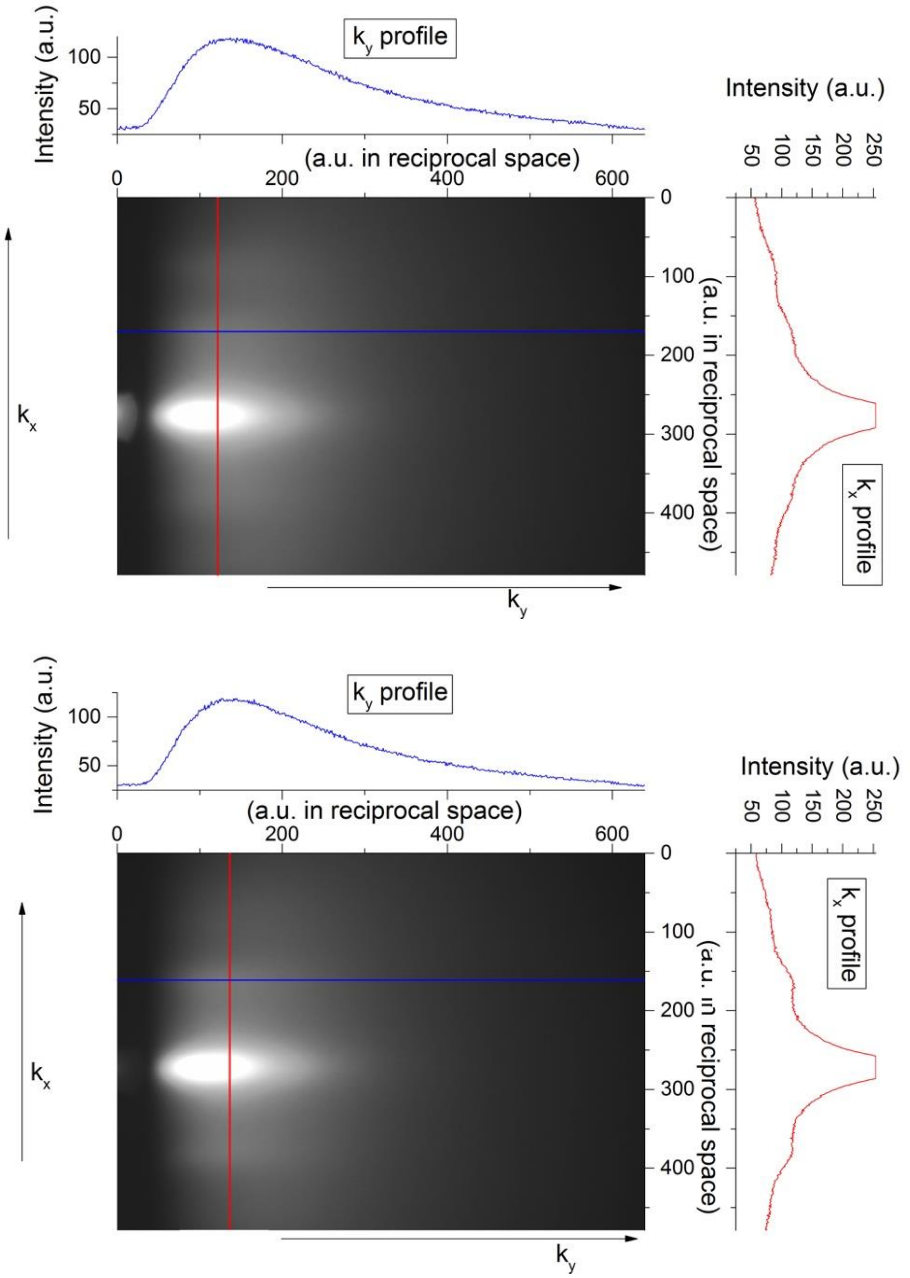

Figure S1-2. RHEED patterns recorded at two different azimuthal angles: ~10^o the top panel) and ~0^o the bottom panel).

Figure S1-3 shows two k_x – profiles taken for different azimuthal angles, plotted together for comparison. For the ideal graphene RHEED pattern should contain either pair of symmetrically placed reflexes corresponding to lattice knots from the first coordination sphere in the reciprocal space or the pair from the second sphere, but always only one pair. (The reflexes from the higher

coordinate spheres are not observable due to the geometrical and intensity issues of the RHEED setup). The presence in the k_x – RHEED profile of graphene two pairs of the peaks means that graphene contains sets of differently in-plane oriented grains (domains). Moreover, the intensity of these peaks depends on the azimuthal angle, which means that these domains have preferable in-plane orientation [1,2]. To explore the exact mutual orientation and relative fraction of the grains full azimuthal scan of the sample is needed. Because of the constructive limitations, the azimuthal angle range is reduced in the case of our set up. However, based on the information from the XRD analysis of copper foil together with RHEED, it can be concluded that graphene contains differently oriented domains with limited azimuthal angle distribution. Since the slope of linear dependency of 2D band on G band positions reveals biaxial strain in graphene (see the main text), we would like to emphasize here that the fact of using "non monocrystalline" graphene in the experiment is not affecting the approach we developed in this work.

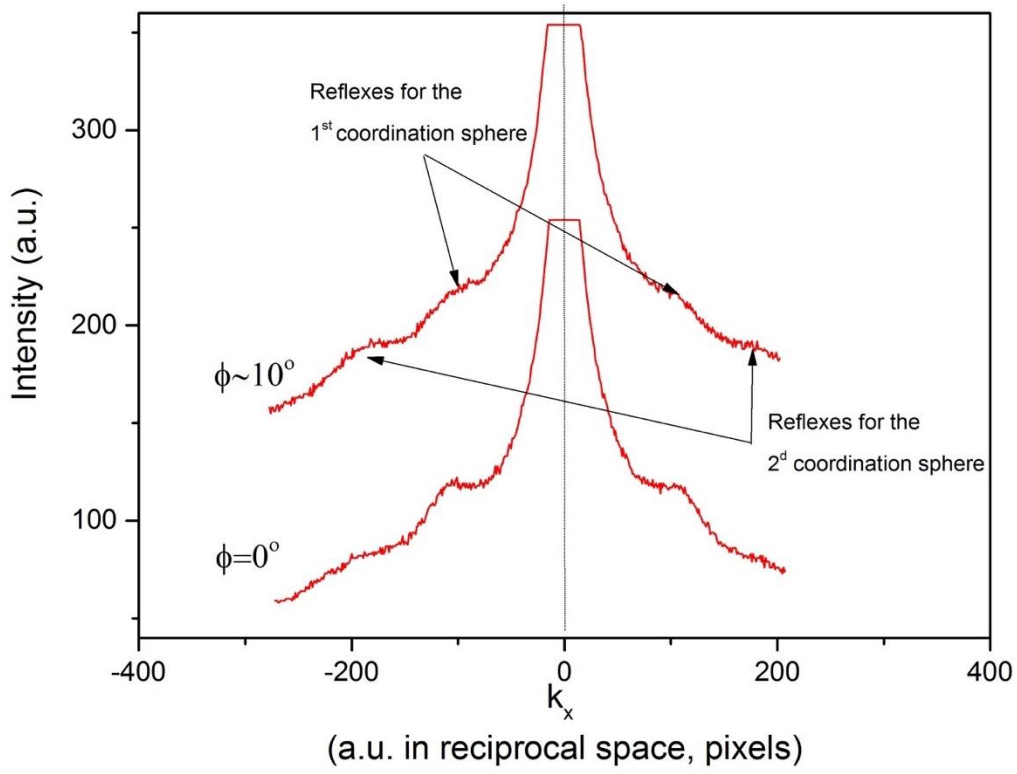

Figure S1-3. RHEED intensity profiles taken for different azimuthal angles (from figure 1S-2).

S2 Determination and characterisation of single layer graphene.

Defect-free structure of the CVD graphene transferred on quartz surface and served as substrate for Bi_2Se_3 deposition is confirmed by the presence of only two Raman active modes, first order G and second order 2D, with the D band intensity at the noise level, in its typical Raman spectrum (Figure S2-1 a) [3,4]. The light transmittance spectra of graphene transferred onto quartz substrate as well as of bare quartz substrate were recorded in the 400–800 nm range using the Proscan MC-121 spectrometer. The diameter of probed area was ≈ 0.5 cm. The light transmittance of the CVD graphene at 550 nm equals to 96.7% (Figure S2-1 b), which is close to the light transmittance value for SLG (97.7%) [5]. Statistical evaluation of the graphene quality was performed using 400 points Raman mapping in the surface areas of 20×20 μm measured in different places of whole transferred graphene sheets through the estimation of intensity ratios of 2D and G bands (I_{2D}/I_G, Figure S2-1 c), mappings of their positions (Figure S2-1 d and e), full width at the half maximum (FWHM) maps of the 2D band (Figure S2-1 f), and corresponding Raman mapping histograms (insets of the Figures S2-1 c-f).

All mapping histograms were fitted with Gauss curve (insets of the Figures S2-1 c-f). All statistical distributions show noticeable maximum corresponding to the SLG fraction, however there is also insignificant fraction of bilayer graphene (BLG). Bimodal distribution of 2D FWHM is more pronounced due to high sensitivity of this parameter to number of layers. Values related to highest peak with maximum at 38.5 cm^{-1} correspond to SLG, the values for another peak (42 cm^{-1}) correspond to BLG [6,7]). As was mentioned above for the most of the SLG area I_{2D}/I_G is close to 2 (Figure S2-1 c, blue colour) and FWHM of 2D band is less than 40 cm^{-1} (Figure S21 f, green colour), which is typical for the CVD-grown on Cu and Ni substrates SLG [6,7]. However, the statistical maximum of 2D band positions is within the range of 2710 – 2725 cm^{-1} (Figure S21 e, blue colour), which indicates a blue shift of 2D band positions relative to ideal undoped and unstrained monolayer graphene (~2700 cm^{-1}) [8,9]. The blue shift was also observed for the position of G band (Figure S2-1 d), which was found to be 1593 cm^{-1} against 1578 cm^{-1} for the ideal undoped and unstrained graphene [8,9] and 1582 cm^{-1} for the SLG transferred on SiO_2 substrate [10]. The blue shifts of the G and 2D positions of the Raman spectra may be associated with mechanical strain and charge doping effects in the graphene/substrate system [8,11].

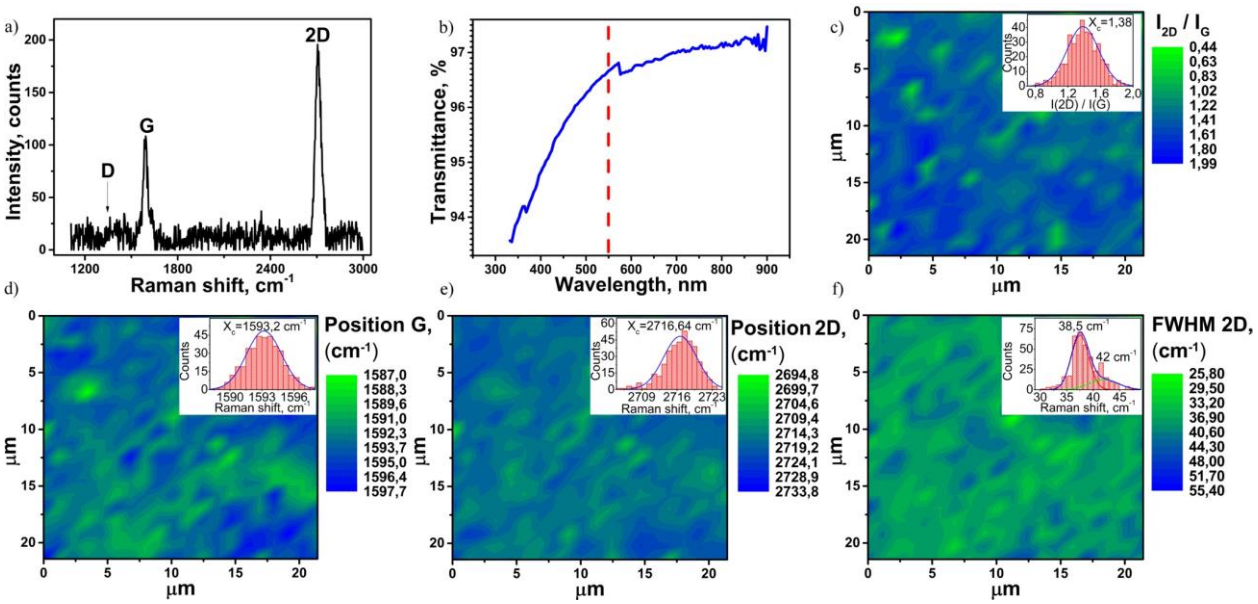

Figure S2-1. a) Raman spectrum of SLG on quartz, the arrow indicates the noise-level D band intensity; b) the transmittance spectrum of SLG on quartz, red dashed line shows 550 nm wavelength; c-f) Raman mapping images of graphene with the corresponding histograms (insets): c) I_{2D}/I_G ratio; d) G band position; e) 2D band position; f) full width at the half maximum (FWHM) of the 2D band. Colour scales represent the amplitude of measured values.

S3 Morphology and thickness analysis of Bi_2Se_3 films probed by AFM.

The whole thickness range (3-400 nm) of the Bi_2Se_3 films used in this work was probed by the AFM technique. In this section (S3) AFM scans (morphological map), RMS roughness and roughness average values, as well as AFM height profiles for films with artificially introduced scratches are collected. Both roughness parameters were obtained using the WSxM scanning probe microscopy software [12]. Figure S3-1 shows the AFM (morphology) maps of substrates (pure quartz (Figure S3-1 a) and quartz/graphene (Figure S3-1 c)), which were used as substrates for the growth of Bi_2Se_3 films. On Figure S3-1 b and d statistical distribution of morphology (height distribution) of the measured surfaces is presented. The blue solid line corresponds to the Gaussian (normal) approximations of these statistical parameters, from which the RMS roughness values were obtained.

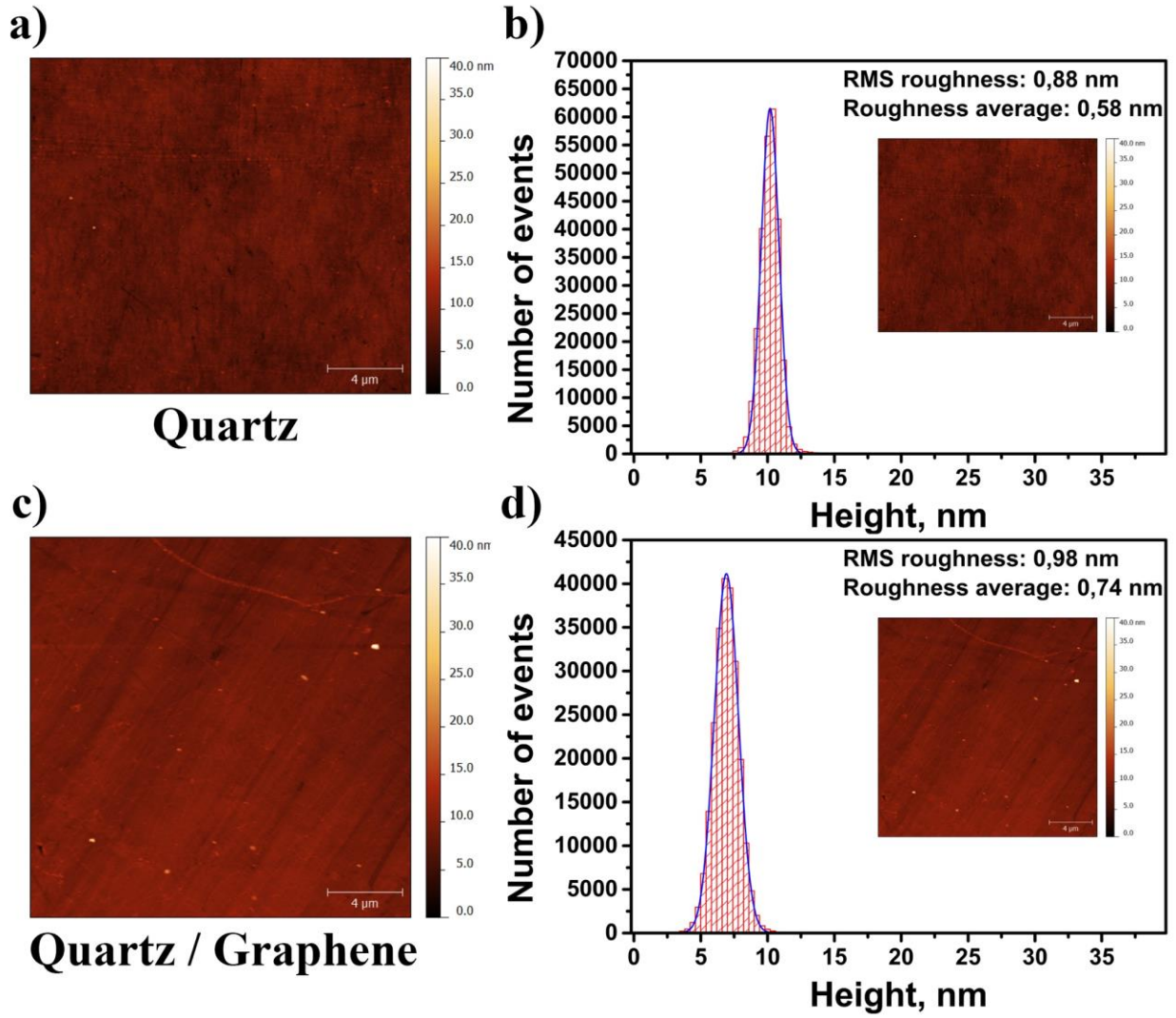

Figure S3-1. a) Atomic force microscope (AFM) image of quartz substrate; b) statistical height distribution of quartz surface fitted with Gaussian curve; c) atomic force microscope (AFM) image of quartz/graphene sample; d) statistical height distribution of quartz/graphene surface fitted with Gaussian curve.

On Figure S3-2 AFM maps with scratches for thickness investigation, height profiles as well as RMS roughness parameters for Bi_2Se_3 films deposited on quartz are presented. Due to the fact that Bi_2Se_3 films with two orders of magnitude of thickness difference (3-400 nm) were used in this work it is difficult to correctly display profiles features of all samples on the same scale. In

Figure S3-2 AFM scans and profiles are shown separately for all films discussed in the paper. The height profiles with ~10 um length are presented in Figure S3-2 to avoid inhomogeneity of film thickness introduced by scratch.

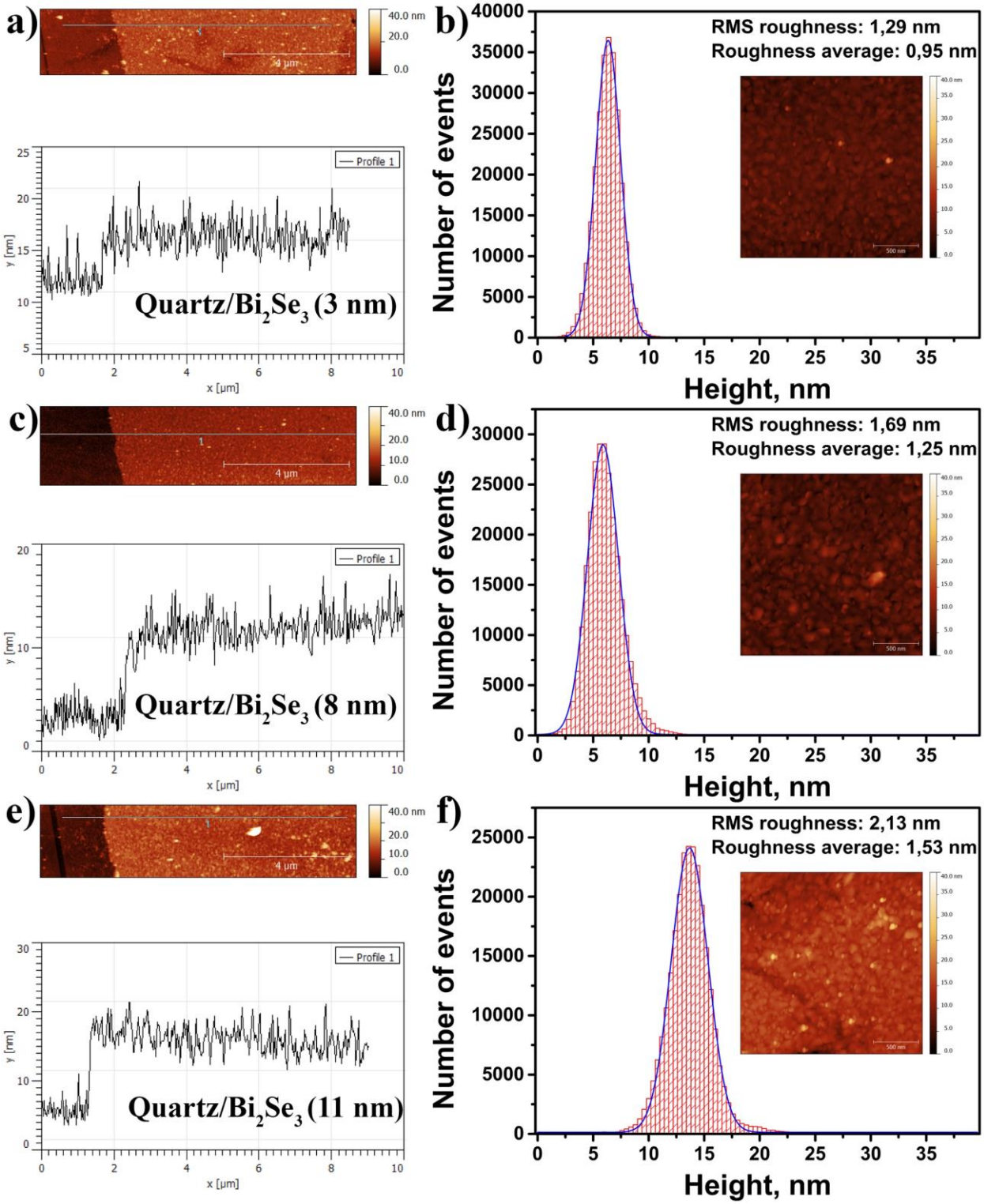

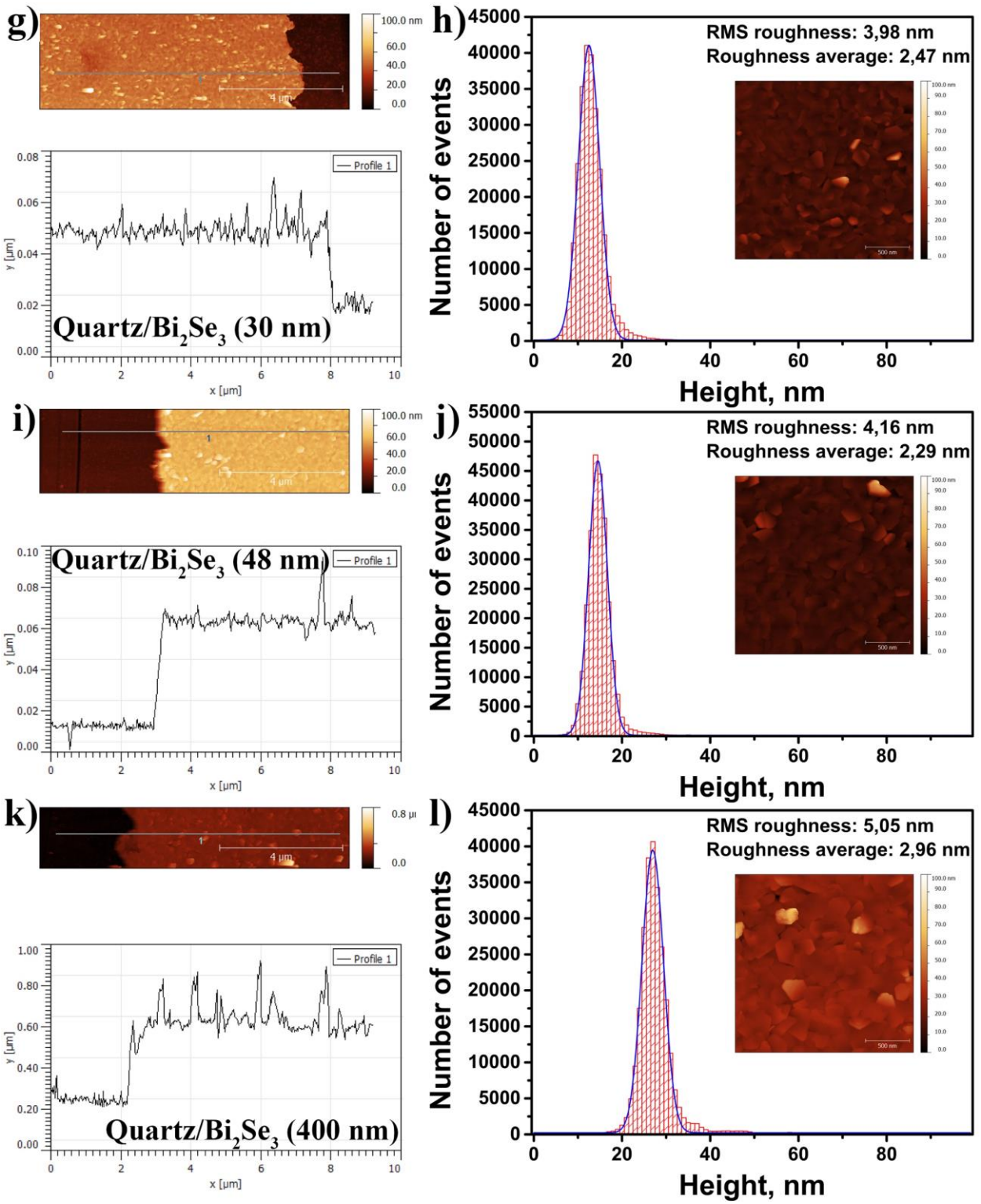

Figure S3-2. a), c), e), g), i), k) Atomic force microscope (AFM) images and height profiles of Bi_2Se_3 films with thickness 3, 8, 11, 30, 48 and 400 nm, respectively, deposited on quartz substrates, artificial scratches were introduced to investigate films thickness; b), d), f), h), j), l) statistical height distributions and its Gaussian fits for 3, 8, 11, 30, 48 and 400 nm Bi_2Se_3 films deposited on quartz.

Figure S3-3 shows AFM maps with scratches for thickness investigated, height profiles as well as RMS roughness parameters for Bi_2Se_3 films deposited on quartz/graphene substrate.

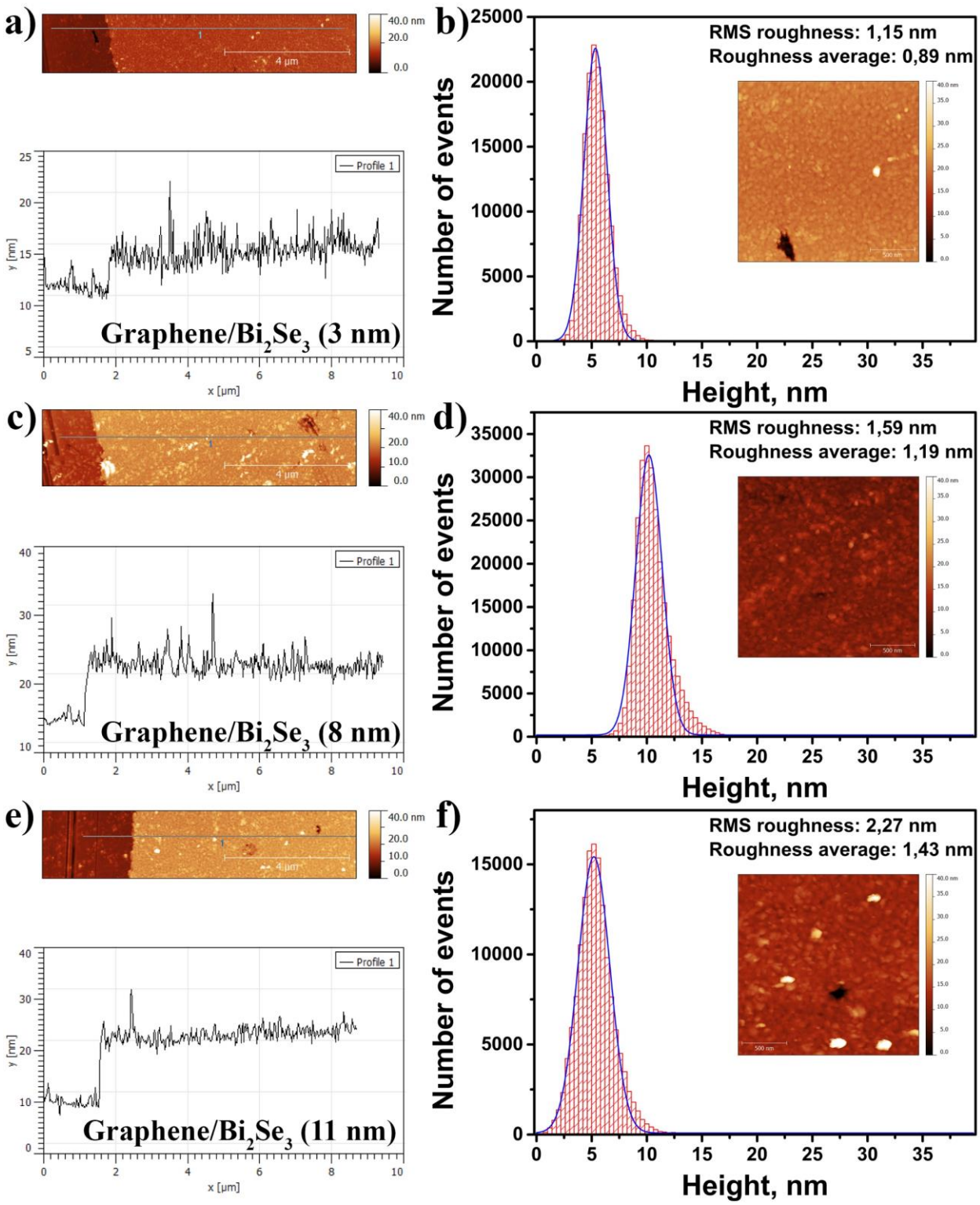
a)
40.0 nm
20.0
0.0
4 µm
Profile 1
y [nm]
x [µm]
Graphene/Bi2Se3 (3 nm)
b)
RMS roughness: 1,15 nm
Roughness average: 0,89 nm
Number of events
Height, nm
c)
40.0 nm
20.0
10.0
0.0
4 µm
Profile 1
y [nm]
x [µm]
Graphene/Bi2Se3 (8 nm)
d)
RMS roughness: 1,59 nm
Roughness average: 1,19 nm
Number of events
Height, nm
e)
40.0 nm
20.0
10.0
0.0
4 µm
Profile 1
y [nm]
x [µm]
Graphene/Bi2Se3 (11 nm)
f)
RMS roughness: 2,27 nm
Roughness average: 1,43 nm
Number of events
Height, nm

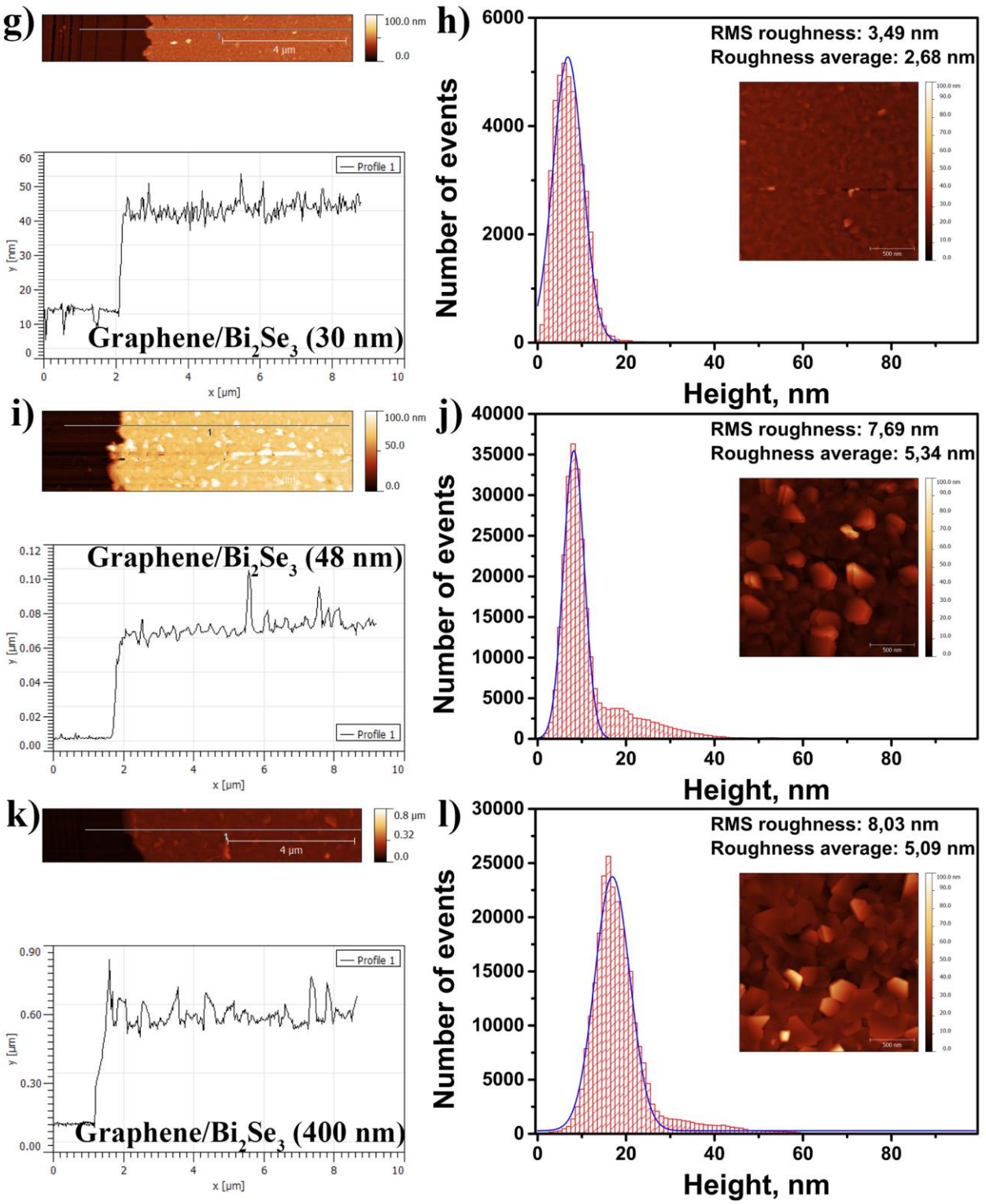

Figure S3-3. a), c), e), g), i), k) Atomic force microscope (AFM) images and height profiles of Bi_2Se_3 films with thickness 3, 8, 11, 30, 48 and 400 nm, respectively, deposited on quartz/graphene substrates, artificial scratches were introduced to investigate films thickness; b), d), f), h), j), l) statistical height distributions and its Gaussian fits for 3, 8, 11, 30, 48 and 400 nm Bi_2Se_3 films deposited on quartz/graphene.

S4 Characterisation of single layer graphene after Bi_2Se_3 films depositions.

As was mentioned above the quality of the CVD graphene transferred on quartz substrate was investigated using Raman technique. As can be seen from Raman spectra of graphene (Figure S1-1 a) the D band intensity, which is responsible for defects, is at the noise level before deposition of Bi_2Se_3 films. The appearance of insignificant D peak of graphene (still close to the noise level) after Bi_2Se_3 films is observed (Figure S4-1 a). Presumably, this can be explained by the formation of defects in graphene due to differences in the lattice parameters of the heterostructure materials.

Figure S4-1 a and b also demonstrate the change in the positions G and 2D after deposition of Bi_2Se_3 films. Such kind of shifts are associated with a change in charge transfer between two layers of heterostructures (see also Figure S4-2), as well as with the strain introduced into the system during the growth process (discussed in more details in the main part).

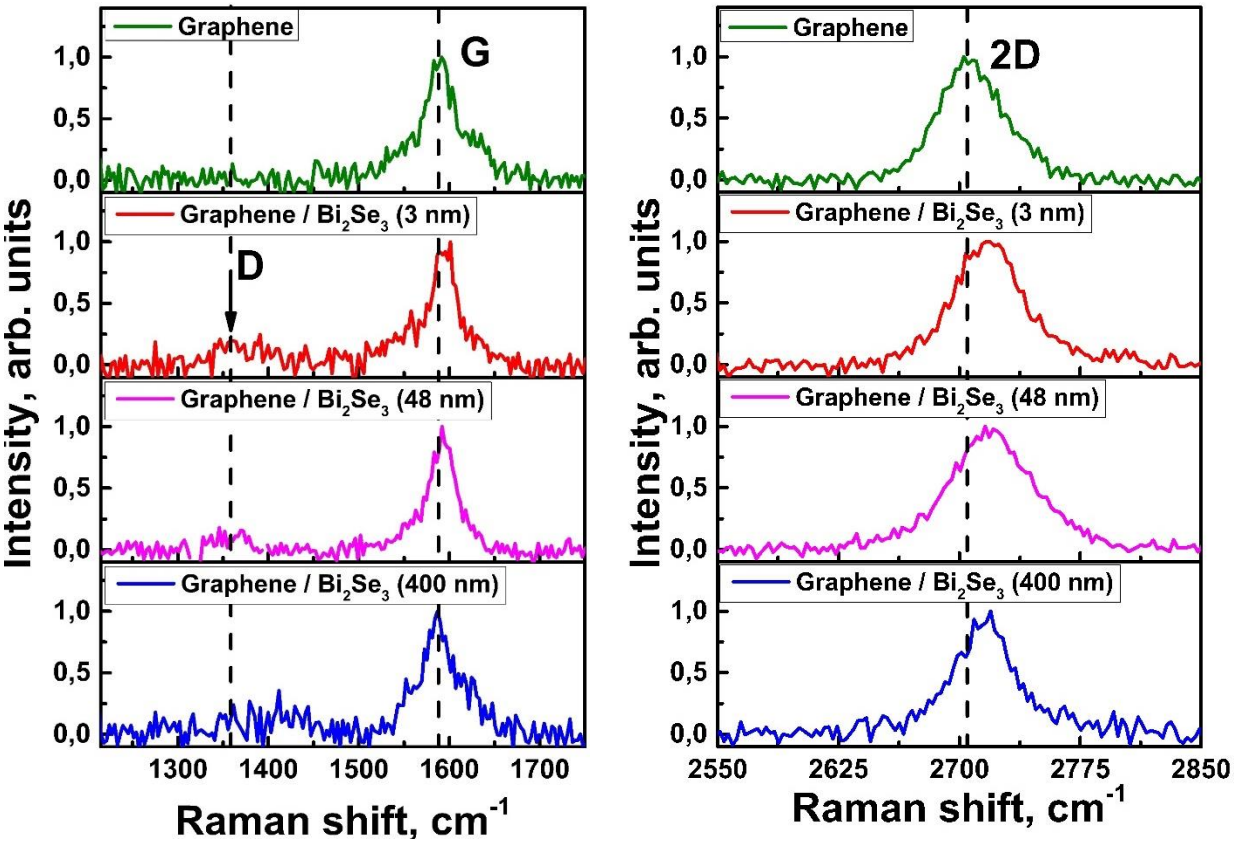

Figure S4-1. a) D, G and b) 2D Raman peaks positions of SLG on quartz and graphene/Bi_2Se_3 films; the arrow indicates the noise-level D band intensity.

Both 2D peaks of Raman spectra graphene/Bi_2Se_3 (3 nm) and graphene/Bi_2Se_3 (400 nm) are shown in Figure S4-2. The 2D peak is asymmetric and fits well with two Voigt peaks. The analysis of such 2D splitting of peaks can be used to estimate changes in the charge density, since such separation of peaks eliminates the influence of deformation and reveals strong correlations between the charge, the position of the peaks and the width of the lines. It is known that a decrease in the splitting of the peak corresponds to an increase in the charge density [13]. This fact shows a different charge transfer (depending on the thickness of the Bi_2Se_3 films), along with the presence of strain in the system. A detailed study of this phenomenon is beyond the scope of this work and is a future direction of research.

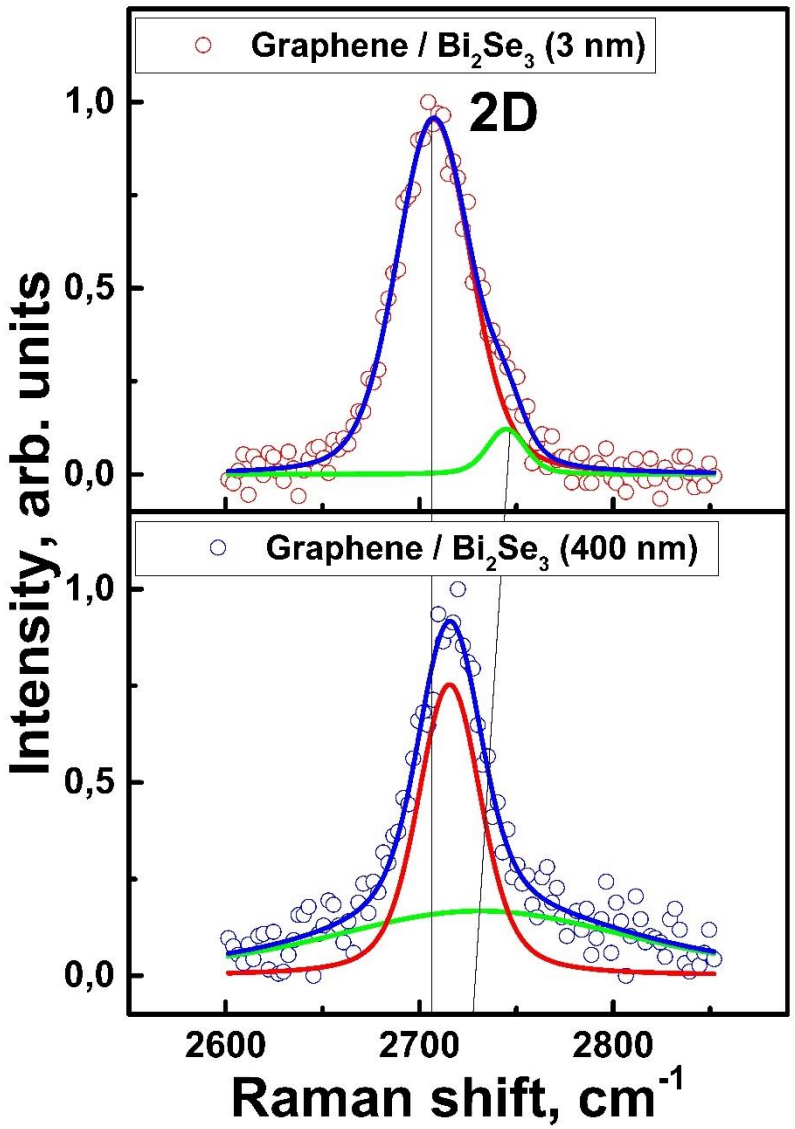

Figure S4-2. The 2D peak of graphene/Bi_2Se_3 (3 and 400 nm) films fitted with two Voigt peaks (lower energy peak (red), the higher energy peak (green)and the envelope (blue)).

S5 Strain distribution in Bi_2Se_3 thick films grown on graphene and quartz substrates.

It should be noted that the scatter of the experimental datapoints along the straight lines with the slope ~ 0.85 for Q/Bi_2Se_3 samples and along the lines with the slopes ~ – 0.85 and ~ 0.85 for the SLG/Bi_2Se_3 heterostructures occurs not only for the Bi_2Se_3 ultrathin films but also for 30, 48 and 400 nm thick films (Figure S5-1 a, b). This means that the strain distribution in the films is maintained for the much longer thickness range then the range reported in the literature, where Bi_2Se_3 films relaxes to the bulk state throughout the few nm [14–17]. This obtained discrepancy can be explained by the significant difference in the kinetics of Bi_2Se_3 films growth between the applied in this work PVD and MBE techniques, revealing that relaxation mechanism in Bi_2Se_3 thin films is very complex problem and requires additional study.

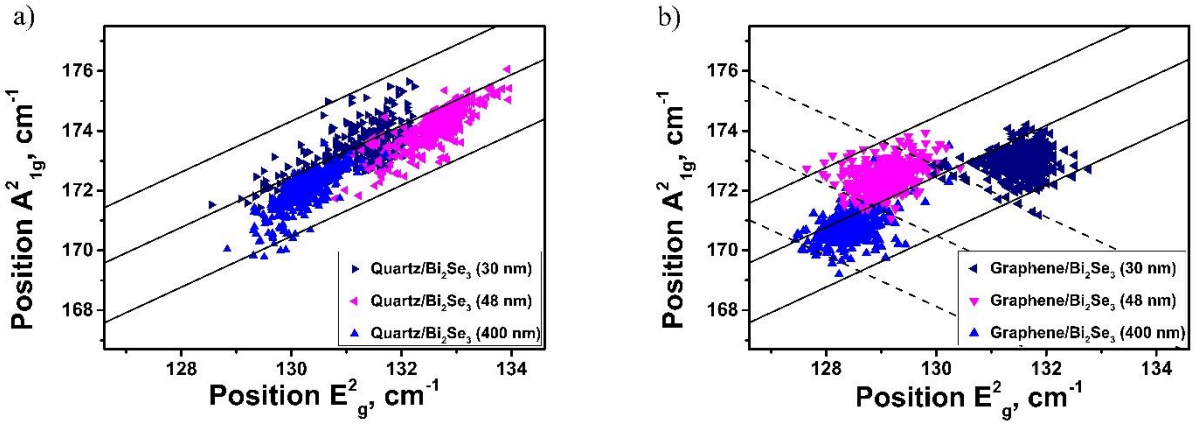

Figure S5-1. The positions of A^2_{1g} band as a function of E^2_g band positions for Bi_2Se_3 thin films deposited on quartz a) and graphene b). Solid lines with the slope of 0.85 correspond to the hydrostatic strain of Bi_2Se_3. The dashed lines with the slope of – 0.85 correspond to the biaxial in-plane tensile strain of Bi_2Se_3 (see the main text for more details).

S6 Crystalline size calculation of 11 nm thick Bi_2Se_3 films grown on graphene.

The crystalline size of 11 nm thick Bi_2Se_3 films grown on graphene was calculated from XRD pattern (for example from 006 reflection (Figure S6-1) using the Debye-Scherrer's equation [18]:

$$D = \frac{k\lambda}{\beta cos\theta},$$

where D is the crystalline size, λ is the wavelength of X-ray (1.540598 Å), k is the shape factor (0.89), θ is the Braggs angle in radians, and $\beta = \frac{\pi}{180} \cdot FWHM$. For this sample D is equal to 10.002 nm, which is in good agreement with AFM thickness measurements (for 11 nm thick Bi_2Se_3 film deposited on SLG).

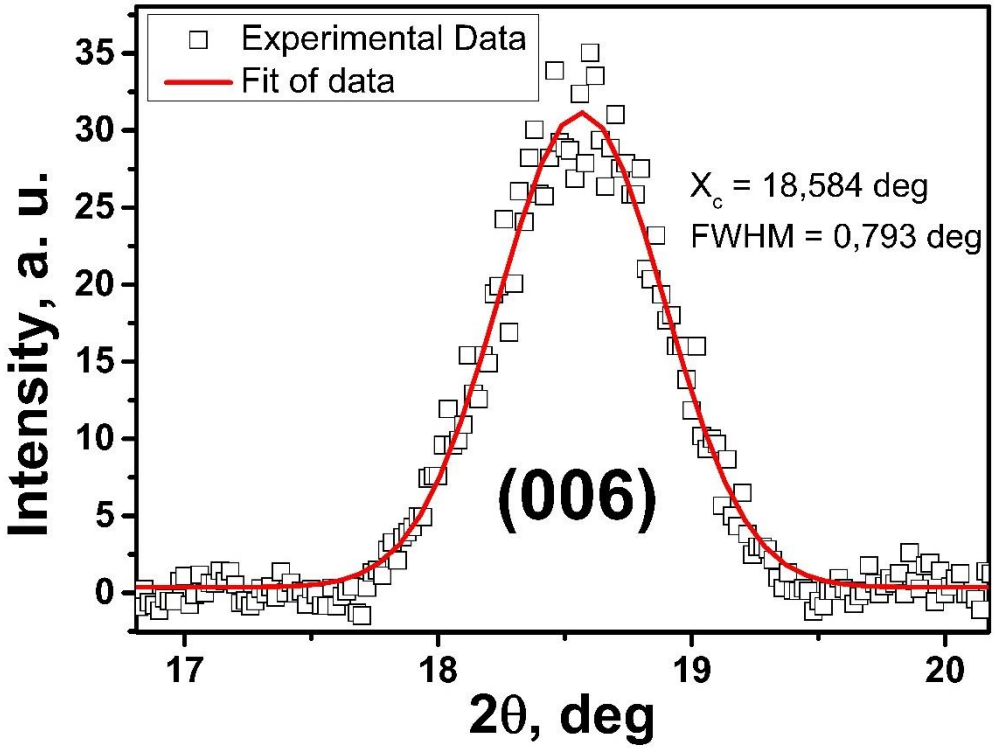

Figure S6-1. 2θ X-ray diffraction pattern (006 peak) of Bi_2Se_3 thin film (11 nm) deposited on SLG.

References:

[1] Lu Z, Sun X, Xiang Y, Washington M A, Wang G C and Lu T M 2017 Revealing the Crystalline Integrity of Wafer-Scale Graphene on SiO_2/Si: An Azimuthal RHEED Approach *ACS Appl. Mater. Interfaces* **9** 23081–91

[2] Xiang Y, Guo F W, Lu T M and Wang G C 2016 Reflection high-energy electron diffraction measurements of reciprocal space structure of 2D materials *Nanotechnology* **27**

[3] Ferrari A C and Basko D M 2013 Raman spectroscopy as a versatile tool for studying the properties of graphene *Nat. Nanotechnol.* **8** 235–46

[4] Casiraghi C, Hartschuh A, Qian H, Pliscanec S, Georgia C, Fasoli A, Novoselov K S, Basko D M and Ferrari A C 2009 Raman spectroscopy of graphene edges *Nano Lett.* **9** 1433–41

[5] Nair R R, Blake P, Grigorenko A N, Novoselov K S, Booth T J, Stauber T, Peres N M R and Geim A K 2008 Fine structure constant defines visual transparency of graphene *Science.* **320** 1308

[6] Losurdo M, Giangregorio M M, Capezzuto P and Bruno G 2011 Graphene CVD growth

on copper and nickel: Role of hydrogen in kinetics and structure *Phys. Chem. Chem. Phys.* **13** 20836–43

[7] Komissarov I V., Kovalchuk N G, Labunov V A, Girel K V., Korolik O V., Tivanov M S, Lazauskas A, Andrulevičius M, Tamulevičius T, Grigaliunas V, Meškinis Š, Tamulevičius S and Prischepa S L 2017 Nitrogen-doped twisted graphene grown on copper by atmospheric pressure CVD from a decane precursor *Beilstein J. Nanotechnol.* **8** 145–58

[8] Berciaud S, Ryu S, Brus L E and Heinz T F 2009 Probing the lntrinsic properties of exfoliated graphene: Raman spectroscopy of free-standing monolayers *Nano Lett.* **9** 34652

[9] Lee J E, Ahn G, Shim J, Lee Y S and Ryu S 2012 Optical separation of mechanical strain from charge doping in graphene *Nat. Commun.* **3** 1-8

[10] Ishigami M, Chen J H, Cullen W G, Fuhrer M S and Williams E D 2007 Atomic structure of graphene on SiO_2 *Nano Lett.* **7** 1643–8

[11] Ni Z H, Yu T, Lu Y H, Wang Y Y, Feng Y P and Shen Z X 2008 Uniaxial strain on graphene: Raman spectroscopy study and band-gap opening *ACS Nano* **2** 2301–5

[12] Horcas I, Fernández R, Gómez-Rodríguez J M, Colchero J, Gómez-Herrero J and Baro A M 2007 WSXM: A software for scanning probe microscopy and a tool for nanotechnology *Rev. Sci. Instrum.* **78** 013705

[13] Wang X, Christopher J W and Swan A K 2017 2D Raman band splitting in graphene: Charge screening and lifting of the K-point Kohn anomaly *Sci. Rep.* **7** 1-9

[14] Kim T H, Jeong K, Park B C, Choi H, Park S H, Jung S, Park J, Jeong K H, Kim J W, Kim J H and Cho M H 2016 Tuning the Fermi level with topological phase transition by internal strain in a topological insulator Bi_2Se_3 thin film *Nanoscale* **8** 741–51

[15] Wang C, Zhu X, Nilsson L, Wen J, Wang G, Shan X, Zhang Q, Zhang S, Jia J and Xue Q 2013 In situ Raman spectroscopy of topological insulator Bi_2Te_3 films with varying thickness *Nano Res.* **6** 688–92

[16] Dang W, Peng H, Li H, Wang P and Liu Z 2010 Epitaxial heterostructures of ultrathin topological insulator nanoplate and graphene *Nano Lett.* **10** 2870–6

[17] Zhao Y, Luo X, Zhang J, Wu J, Bai X, Wang M, Jia J, Peng H, Liu Z, Quek S Y and Xiong Q 2014 Interlayer vibrational modes in few-quintuple-layer Bi_2Te_3 and Bi_2Se_3 two-dimensional crystals: Raman spectroscopy and first-principles studies *Phys. Rev. B - Condens. Matter Mater. Phys.* **90** 245428

[18] Cullity B D and Weymouth J W 1957 Elements of X-Ray Diffraction *Am. J. Phys.* **25** 3945